JGR Space Physics

RESEARCH ARTICLE
10.1029/2019JA027286

Reverse Fountain and the Nighttime Enhancement in the Ionospheric Electron Density Over the Equatorial Region: A Case Study

Sneha Yadav[1,2], R. K. Choudhary[1], Jyoti Kumari[1,3], Surendra Sunda[4], P. R. Shreedevi[1,5], and Tarun. K. Pant[1]

[1]Space Physics Laboratory, Vikram Sarabhai Space Centre, Trivandrum, India, [2]Institute for Space-Earth Environmental Research, Nagoya University, Nagoya, Japan, [3]Department of Applied Physics, Amity Institute of Applied Sciences, Noida, India, [4]GNSS R&D Centre, Airport Authority of India, Ahmedabad, India, [5]School of Space and Environment, Beihang University, Beijing, China

Key Points:
- We investigated the occurrence characteristics and mechanism of ionospheric nighttime enhancement over the equatorial region
- SBAS-generated 2D-TEC maps are used to visualize the reverse fountain effect over the Indian region
- Ionospheric nighttime enhancement over the equatorial regions are associated with the plasma motions caused by the retreating anomaly

Correspondence to:
S. Yadav,
sneha.yadav84@gmail.com

Citation:
Yadav, S., Choudhary, R. K., Kumari, J., Sunda, S., Shreedevi, P. R., & Pant, T. K. (2020). Reverse fountain and the nighttime enhancement in the ionospheric electron density over the equatorial region: A case study. *Journal of Geophysical Research: Space Physics*, *124*, e2019JA027286 https://doi.org/10.1029/2019JA027286

Received 12 AUG 2019
Accepted 6 APR 2020
Accepted article online 14 APR 2020

Abstract This paper focuses on the linkage between reverse fountain effect and anomalous enhancement in the nighttime electron density over the equatorial ionosphere often referred as the ionospheric nighttime enhancement (INE). The Global Positioning System (GPS)-derived total electron content (TEC) measurements over two Indian equatorial stations and ionosonde measurements are used to investigate the occurrence characteristics and mechanism of the premidnight and postmidnight INE events. The high-resolution spatiotemporal two-dimensional (2D) TEC maps generated by using satellite-based augmentation system are used to visualize the reverse fountain effect. These TEC maps are found to be effective in envisaging the motion of equatorial ionization anomaly (EIA) in nighttime ionosphere and its impact on the distribution of electron density over the equatorial region. Salient features of this case study illustrate that, accompanying enhancements in the nighttime TEC, there exist decrease in the F2 layer height, prevalence of downward vertical plasma drift, and dramatic increase in the F2 region electron density. The 2D-TEC maps reveal the persistence of well-developed EIA until late evening hours and its gradual shift toward equator during the events of postmidnight INEs. It is found out that the premidnight INE is not invariably linked to the prereversal enhancement of the zonal electric field and could be associated with the redistribution of electron density caused by the reverse fountain effect. The present observations indicate that although the westward electric field serves as a prime driver, the INEs over the equatorial regions are associated with plasma motions caused by the retreating anomaly.

1. Introduction

Understanding the evolution of nighttime ionospheric electron density remains an elusive aspect in spite of the extensive research over the past several decades. At nighttime, during the absence of production of ionization, the ionospheric electron density is generally expected to decay gradually, but it does not behave as predicted by the simple notion and show enhancement occasionally. This phenomenon is called as the ionospheric nighttime enhancement (INE), and it depends strongly on location, season, and level of solar and geomagnetic activity. Several studies have been conducted to understand the statistics and the physical processes involved in the INE using the total electron content (TEC) of the ionosphere, peak plasma density of F-region (foF2/NmF2), tomographic images, and radio occultations over midlatitudes and low latitudes (Janve et al., 1979; Balan & Rao, 1987; Lois et al., 1990; Bailey et al., 1991; Balan et al., 1994; Su et al., 1994; Mikhailov, Förster, & Leschinskaya, 2000; Dabas & Kersley, 2003; Farelo et al., 2002; Pavlov & Pavlova, 2007; Luan et al., 2008; Liu et al., 2013; Le et al., 2014; Jiang et al., 2016). Based on the time of occurrence, the INEs have been classified into two types, namely, postsunset/premidnight and postmidnight. Further, according to the geographic region, they can also be categorized into midlatitude and low-latitude INEs. The underlying physical mechanism proposed for different INE events, however, are different.

The INE events over midlatitudes are generally considered as a consequence of the increase of electron density from the downward plasma fluxes from plasmasphere (Mikhailov, Leschinkaya, & Förster, 2000; Farelo et al., 2002; Dabas & Kersley, 2003). At low latitudes, the prereversal enhancement (PRE) of the eastward

electric field and consequent upward E × B drift, which raises the evening equatorial-F region to higher altitudes, is recognized as the primary mechanism for the postsunset/premidnight enhancements of TEC (Bailey et al., 1991; Su et al., 1994, 1995; Balan & Bailey, 1995; Balan et al., 1995). However, the mechanism for the postmidnight enhancements are yet to be identified unambiguously and is a topic of investigation. Liu et al. (2013) brought out the essential role of the westward electric field in forming the postmidnight enhancements in electron density of ionospheric F layer over low latitudes. Further, the simulation studies carried out by Le et al. (2014) demonstrated that the downward E × B plasma drift due to westward electric field at night is the main driving force for the nighttime enhancement and the delayed westward electric field can produce significant postmidnight enhancement over low latitudes. However, the observations from the equatorial region supporting this simulation results are still lacking. Further, Jiang et al. (2016) suggested the crucial role of vertical E × B drift along with meridional wind in causing the postmidnight electron density enhancement over both equatorial and low latitudes. The inconsistent results between modeling and different observations may be associated with some physical mechanism which remains unraveled till now. Also, it is worth mentioning that unlike the INE at midlatitude and low latitude, less attention has been paid to the equatorial region where equatorial electrodynamics plays a dominant role.

The nighttime equatorial ionosphere is known for the existence of equatorial plasma bubbles and reverse fountain effect (Woodman and Lahoz, 1976; Sridharan et al., 1993). The reverse fountain effect is a consequence of the change in the direction of the zonal electric field from eastward to westward and characterized by the movement of the equatorial ionization anomaly (EIA) crest toward the equator. In general, there are extensive studies in the literature on the generation and manifestation of equatorial plasma bubbles. However, surprisingly, the studies related to the reverse fountain and its impact on the electron density distribution over the equatorial ionosphere are rather sparse. Sridharan et al. (1993) provided the first visual representation of the reverse equatorial plasma fountain during nighttime using All Sky Imaging Fabry-Perot Spectrometer. Thereafter, Mukherjee (2002) and Narayanan et al. (2013) also touched upon this aspect with all-sky imaging observations. However, studies pertaining to the effect of this changing electrodynamics on the nighttime electron density distribution over the equatorial ionosphere remain inconclusive. This could partly be due to the lack of measurements from closely separated locations covering the entire EIA region. Further, the studies pertaining to the variability of EIA were mostly based on a single or a set of ground-based measurements along a particular meridian and therefore suffer from the constraint in providing the comprehensive visualization on the motion of EIA.

In this context, a recently developed novel and cost-effective technique to generate two-dimensional (2D) TEC maps using satellite-based augmentation system (SBAS) platform (Sunda et al., 2015) achieves significance. The technique utilizes the SBAS-broadcasted ionospheric vertical delay to generate the 2D-TEC maps. The advantage of this technique is that just by using a single SBAS-enabled receiver, the TEC maps can be generated over the entire region served by the SBAS. These SBAS-generated TEC maps have been shown to be very effective in studying the evolution/subsidence of daytime EIA during different space weather conditions (Yadav et al., 2016).

The present work focuses on investigating the enhancement in the ionospheric electron density during nighttime over the equatorial region. The 2D-TEC maps covering the Indian longitudes have been used for the first time to visualize the reverse fountain effect and to provide its linkage with the INE events in the equatorial ionosphere. The study also sheds light on the underlying physical mechanisms which are plausibly responsible for INE events over the equatorial region.

2. Data Set

The Global Positioning System (GPS)-derived TEC measurements over the two Indian stations Trivandrum (8.5°N, 77.1°E, 0.5°N dip latitude) and Bangalore (12.9°N, 77.6°E, 4.1°N dip latitude) have been used to study the INE events. Trivandrum is a dip equatorial station, whereas Bengaluru lies just outside the equatorial electrojet zone. The time period of the study is during January–February 2014 because of the availability of simultaneous data from GPS and a colocated digital ionosonde at Trivandrum.

The information on bottom side ionosphere has been derived from the Digisonde (DPS-4D) operating at Trivandrum. The bottomside ionospheric parameters are extracted from the ionogram by manual scaling, which are available at the resolution of 7.5 min. The key parameters used in this study are critical

frequency of the F2 layer (foF2), height of the peak electron density in F2 layer (hmF2), and base height of the F layer (h′F). The F region vertical drift velocity (Vz) is obtained using the Drift Explorer software package developed at UMLCAR (Reinisch et al., 2005 and references therein). The Drift Explorer processing software is based on Digisonde Drift Analysis technique to estimate the plasma drift in three directions by using the observations of line-of-sight velocities (Doppler frequency shifts) of the sky map source points (Scali et al., 1997). It is to be noted here that the parameters obtained from ionograms are not used during the presence of spread-F.

The Indian SBAS-GAGAN (GPS-Aided Geo Augmented Navigation) is the first SBAS system to serve over equatorial and low-latitude regions. It broadcasts the ionospheric corrections at L1 frequency in the form of vertical delay at the predefined ionospheric grid points (IGPs). The GAGAN is broadcasting the ionospheric vertical delay at 102 IGPs over the Indian subcontinent at a spatial resolution of 5° × 5°. By using SBAS-enabled GPS receivers, the information on these Grid Ionospheric Vertical Delay over the entire region served by SBAS can be received in the form of the messages. These messages have been decoded to generate the 2D-TEC maps over the Indian longitudes by using the methodology described by Sunda et al. (2015).

3. Results

Before understanding the underlying physical processes causing the INE, it is prerequisite to understand its occurrence characteristics. The nighttime enhancement in TEC is a regular feature over equatorial and near equatorial stations and is found to occur frequently during winter and equinox. During February 2014, the INE was present almost 80% of the nights. Figure 1 depicts typical examples of INE observed over Trivandrum and Bangalore for four different days in February 2014. It can be seen from the figure that after achieving the daytime peak at ~10 UT (1530 LT), the TEC values showed gradual decay till 14 UT (2030 LT). The TEC values again began to increase from ~1500 UT and a hump of enhanced TEC occurred at 16–22 UT (2130–0330 LT), which is referred as the INE. The TEC values at Bangalore appeared to be higher as compared to those in Trivandrum from 0530 UT (1100 LT) to premidnight hours. The variability in the day-to-day occurrence characteristics and structure of INEs is well discernible from the figure. We may however note from Figure 1 that the magnitude of INE does not remain constant and there remains a large day-to-day variability. Nighttime TEC shows a large enhancement of the order of 10–15 TECU on 1 and 6 February 2014, whereas on 21 and 22 February 2014, only the presence of two small humps in the nighttime is observed.

The next step was to identify the magnitude of INE, and for this, two types of criteria have been suggested in the previous works. The exponential decaying values were treated as the background reference by Young et al. (1970) to identify INE (Criterion 1). Liu et al. (2013) used the preceding minimum values after sunset as a reference to examine the nighttime enhancement (Criterion 2). Liu et al. (2013) evaluated both criteria and suggested that using preceding minimum values after sunset (Criterion 2) as a reference is better and more convenient to deal with as compared to the Criterion 1. Therefore, we have adopted Criterion 2 to identify the INE events in the present study. While Liu et al. (2013) employed this technique in foF2, we use it to identify the INE events in TEC. Since both TEC and foF2 correspond to the ionospheric density, it should not affect the identification of the INE events whether the technique is employed in TEC or foF2. The nighttime TEC values are then subtracted from this reference values to get ΔTEC values, which represent the magnitude of nighttime enhancement.

To study the background ionosphere under which the INE occurs in TEC, the resulting ΔTEC values have been plotted along with different bottomside ionospheric parameters derived from ionosonde operating at Trivandrum. This paper presents three cases to understand the occurrence characteristics and underlying mechanism for the INEs. A case wherein INE was absent is also presented for better understanding. It is worth mentioning here that the absence of equatorial spread-F was also one of the criteria for selecting the days for this case study as the derived bottomside ionospheric parameters from ionosonde during equatorial spread-F remain unreliable. Figures 2, 4, 6, and 8 depicts the temporal variation of nighttime ΔTEC values for both the station (a), along with foF2 (b), hmF2 (c), h′F (d), and Vz (e) at Trivandrumfor 01 February, 21 February, 06 February, and 20 February, respectively. The cyan color vertical bars in panel (e) depict standard deviation for vertical drift. As described earlier, nighttime equatorial ionosphere is

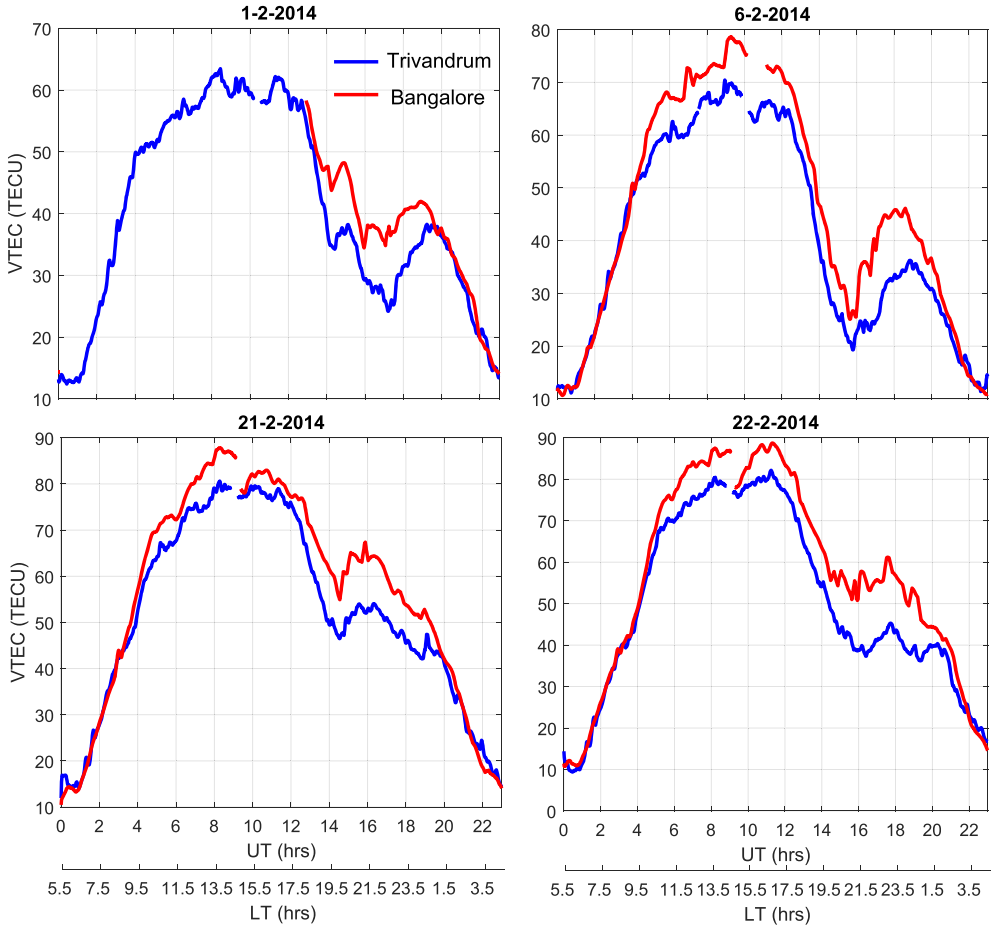

Figure 1. Temporal variation of TEC displaying the typical examples of ionospheric nighttime enhancement over Trivandrum and Bangalore.

known for the existence of the reverse fountain effect when the crest of anomaly retreats back toward the equator. Therefore, in order to visualize the reverse fountain and its effect on the electron density distribution in the nighttime ionosphere, the 2D-TEC maps generated by using SBAS platform have been shown in Figures 3, 5, 7, and 9 for 01 February, 21 February, 06 February, and 20 February 2014, respectively. The location of Trivandrum and Bangalore in the 2D maps are depicted by circle and square symbol, respectively.

3.1. Case1: 01 February 2014

Figure 2 depicts the variation in ΔTEC at two stations during 13–23 UT (1830–0430 LT) along with other ionospheric parameters on 01 February 2014. The presence of two humps in the ΔTEC values during premidnight and postmidnight hours can be identified from Figure 2. The first enhancement at ~14–16 UT (1930–2130 LT) is found to occur immediately after the sudden increase in the F-region height (both h′F and hmF2). The high values of h′F (~340 km) and hmF2 (~400 km) and positive vertical drift (~40 m/s) during 13–14 UT (1930–2030 LT) indicate the presence of PRE of the zonal electric field. The vertical drift becomes downward or achieves negative values during 16–19 UT with a maximum value of approximately −30 m/s. It is worth noting that the postmidnight enhancement in the ΔTEC at ~1730–21 UT (23–0230 LT) began immediately after the downward turning of the vertical drift. The foF2 values, which did not show much variability during premidnight, show an abnormal jump of ~6 MHz from ~1730 UT to 19 UT (23–0130 LT), marking the appearance of postmidnight INE. The h′F and hmF2 were also found to reduce significantly during this time, achieving the lowest values of ~220 and ~ 300 km, respectively. The postmidnight INE as seen in the ΔTEC values was higher over Trivandrum as compared to Bangalore, which is in contrast to that observed in the TEC values (Figure 1). This shows the importance of using ΔTEC values over TEC values in examining the magnitude of INE. It is interesting to note that majority of the features in ΔTEC

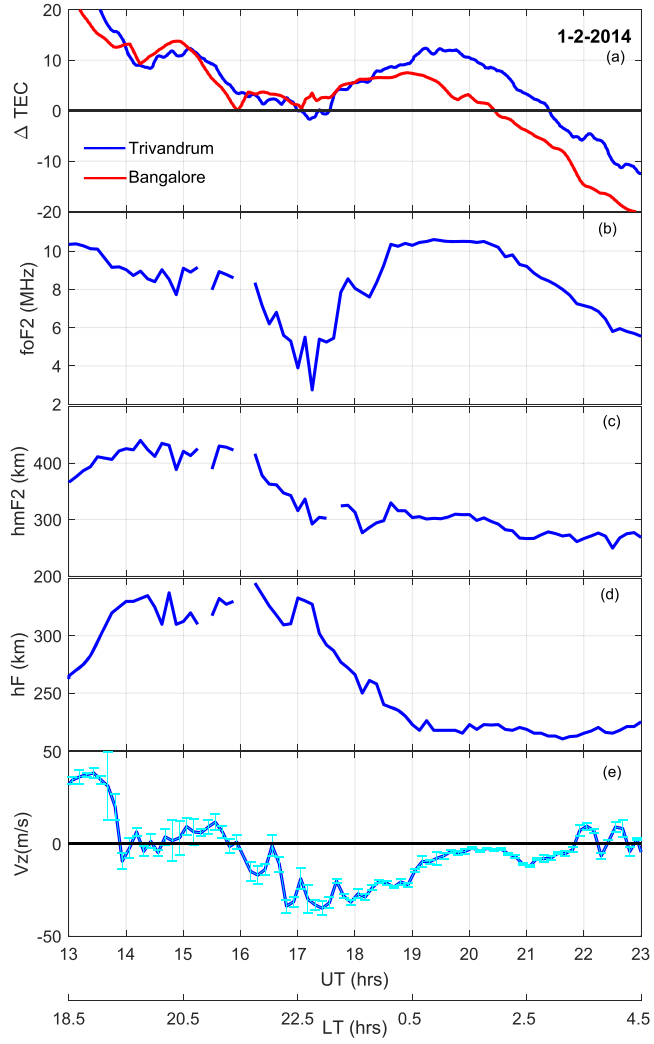

Figure 2. Temporal variation of nighttime ΔTEC values for Trivandrum and Bangalore (a), along with foF2 (b), hmF2 (c), h′F (d), and Vz (e) at Trivandrum for 01 February 2014. The cyan color vertical bars in panel (e) depicts standard deviation for vertical drift.

exhibited by Bangalore is also observed over Trivandrum but with a certain time delay in the postmidnight hours. The ΔTEC values over Bangalore began to increase from 17 UT and peaked at ~18–19 UT. The enhancement over Trivandrum was observed with a delay of 30 min, that is, from 1730 UT and maximized at ~19–20 UT. The ΔTEC values were higher over Trivandrum (maximum value was ~11 TECU) and persisted for a longer time as compared to those over Bangalore (maximum value was ~8 TECU).

Figure 3 displays the time sequence 2D-TEC images on 01 February 2014 during 14–21 UT (1930–0230 LT). The TEC values are represented through a color code. It can be seen from Figure 3 that these 2D maps encompassed a large latitudinal (5°S to 45°N) and longitudinal (55–110°E) area over the Indian longitudes and appeared to be effective in visualizing the reverse fountain effect. Although these images are available at a time resolution of 5 min, the present study does not require such high-cadence data. We have shown the 2D-TEC maps at a resolution of 1 hr. The increased electron density can be seen between 10°N and 20°N at 14 UT (1930 IST), indicating the presence of crest of ionization in the evening sector. As time progressed, the anomaly gets weakened, the electron density decreased, and the crest tended to move toward lower latitudes. This indicates the subsidence of EIA or the reverse fountain effect. It can be noted that the crest of ionization was centered at ~10°N during ~18–19 UT. This exactly coincides with the time of occurrence of peak ΔTEC values over Bangalore and Trivandrum (see Figure 2). At 20 UT (0130 LT), the increased electron densities moved further southward and were also observed to be shifted toward western longitude sector. At ~2100 UT (0230 IST), no spatial structures in electron density were present and low values of TEC prevailed over the entire region, indicating the complete absence of anomaly. The ΔTEC values as seen in Figure 2 also showed a similar feature and began to decrease sharply after 20 UT. These results suggest that the features seen in 2D-TEC maps show a close semblance with the structures observed in the ΔTEC values over the individual stations.

3.2. Case 2: 21 February 2014

The nighttime variation of ΔTEC values over Trivandrum and Bangalore on 21 February 2014 is presented in Figure 4. It is observed that during the premidnight sector (15–17 UT or 2030–2230 LT), the ΔTEC values showed an enhancement of ~10 TECU. This premidnight INE was accompanied by the abrupt decrease in the F-region height and negative Vz observed during 1430–1600 UT. The ΔTEC values decreased gradually after 17 UT, and later, a slight increase of ~3TECU during the postmidnight sector (19–20 UT or 0030–0130 LT) was observed over Trivandrum. The h′F and hmF2 over Trivandrum began to decrease gradually after the enhancement at 14 UT. The vertical drift did not show any considerable change after 16 UT. In contrast to the behavior of TEC, foF2 show a gradual increase from 15 UT to 20 UT, exhibiting an enhancement of ~3 MHz.

The 2D-TEC images between 14 and 21 UT for 21 February 2014 are shown in Figure 5. The sharp crest of ionization in the 2D-TEC maps at 14–15 UT (1930–2030 LT) between 15°N and 20°N is well discernible from Figure 5. The effect of downward vertical drift at 14–16 UT (Figure 4) is observed in the 2D-TEC maps in terms of rapid decrease in the EIA crest magnitude at 16–17 UT (Figure 5). Interestingly, the gradient between the electron density at the crest and trough also reduced significantly during this time, suggesting redistribution of ionization toward the equator. The ΔTEC values in Figure 4 also show an enhancement at 15–17 UT (2030–2230 LT). This clearly suggests that the premidnight enhancement over the equatorial region occurred primarily because of the prevalence of downward drift, which is prerequisite for the reverse fountain effect causing redistribution of ionization, as observed in this case. At 18 UT, enhanced plasma density was observed at

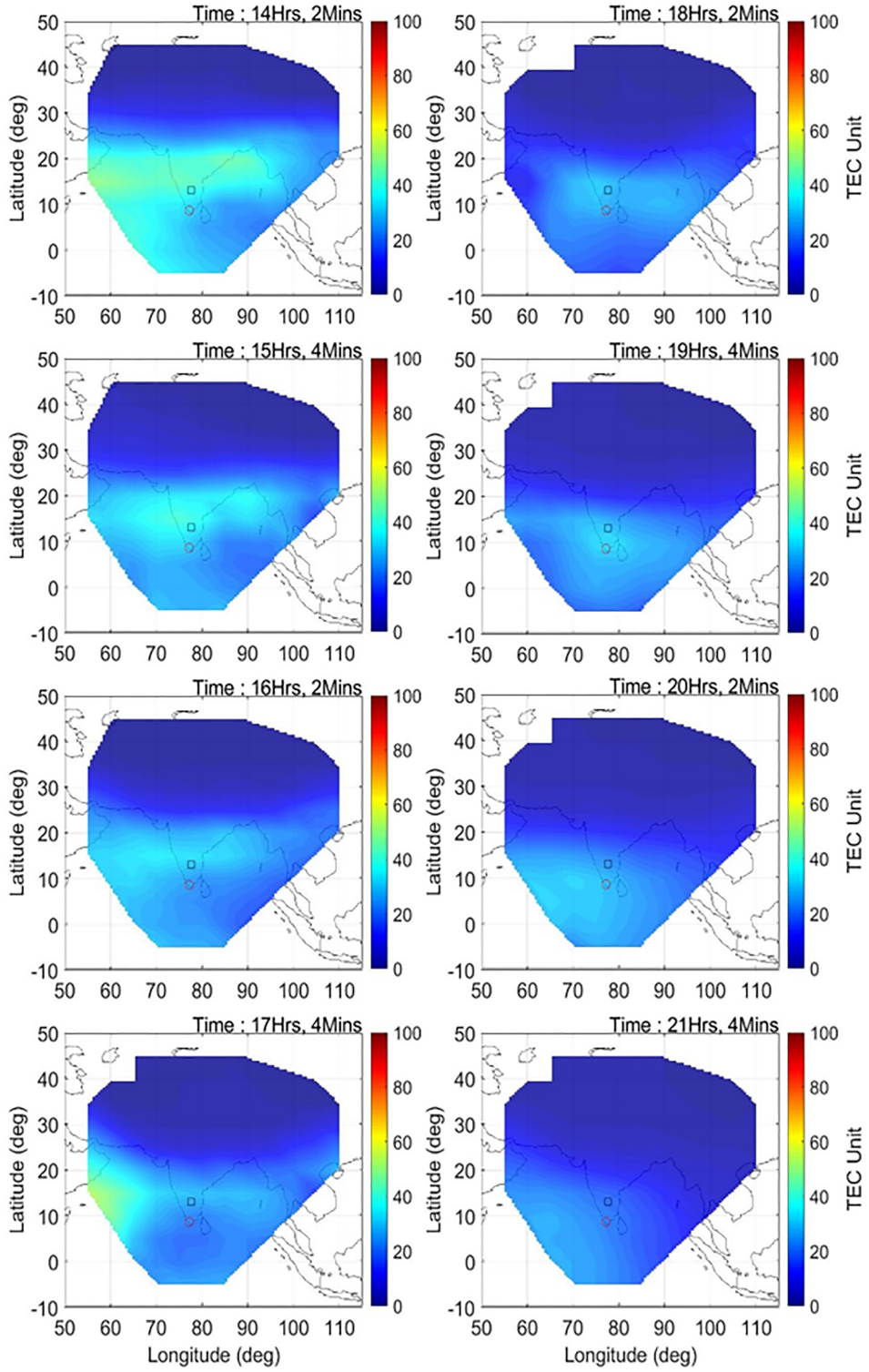

Figure 3. The 2D-TEC maps generated by using SBAS (satellite-based augmentation system) for 01 February 2014. The TEC values are represented through a color code. The location of Trivandrum and Bangalore in the maps are depicted by circle and square symbol, respectively.

around 8–15°N, which decay gradually as time progressed with EIA crest also moved southward. The relatively increased plasma density at ~10°N during 20–21 UT as seen in the TEC maps (Figure 5) appeared around the same time when the postmidnight hump in the ΔTEC values was observed in Figure 4.

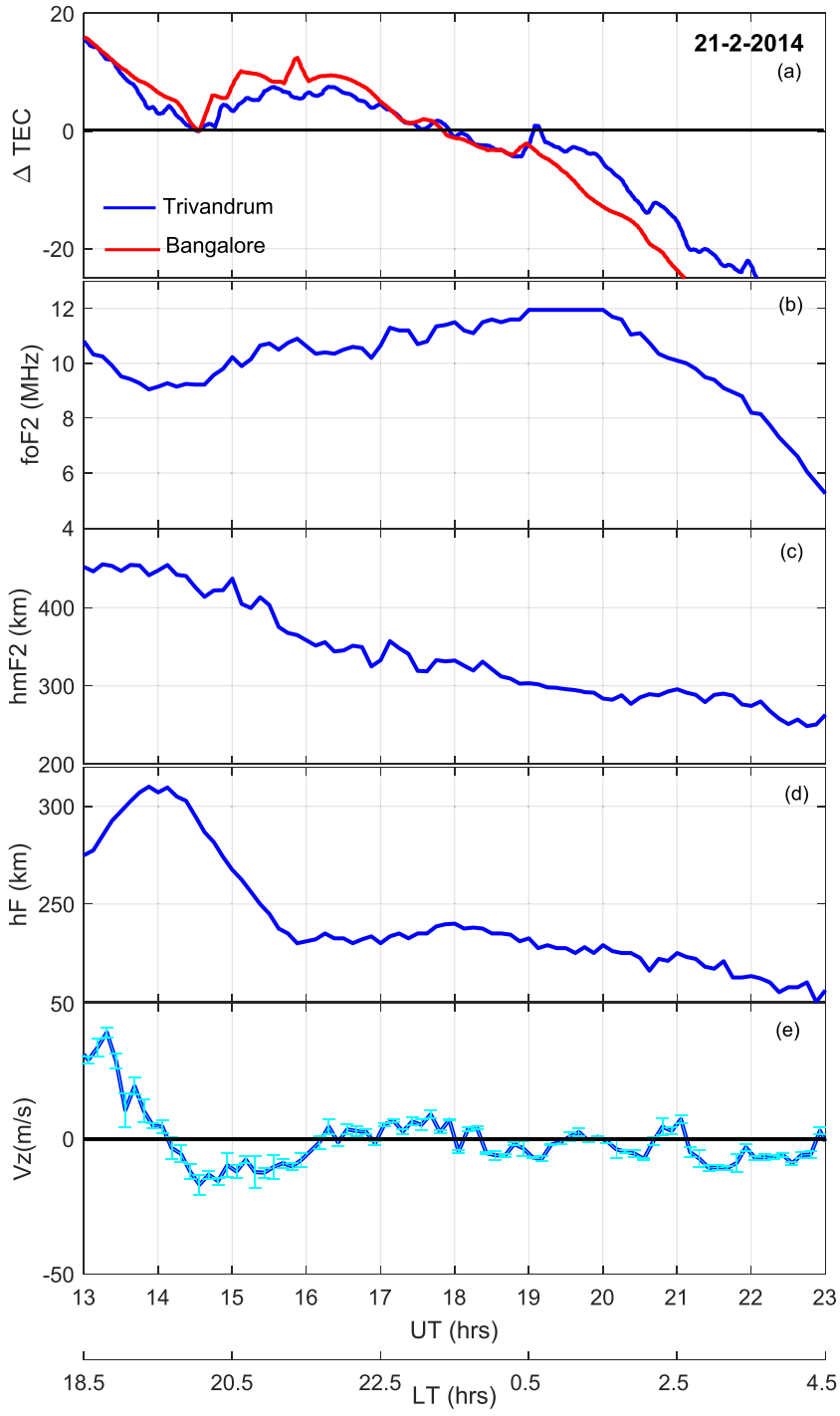

Figure 4. Same as Figure 2 but for 21 February 2014.

3.3. Case 3: 06 February 2014

On 6 February 2014, a large enhancement in the ΔTEC values (~15–20 TECU) during ~16–21 UT (2130–0230 LT) over both stations was observed (see Figure 6). The INE structure persisted for 5 hr covering both pre-midnight to postmidnight sector. The enhancement occurred first over Bangalore with higher ΔTEC values as compared to Trivandrum. The foF2 values (~5 MHz) showed a sharp increase during this time; however, the magnitude of such enhancement remained indiscernible because of the presence of spread-F during

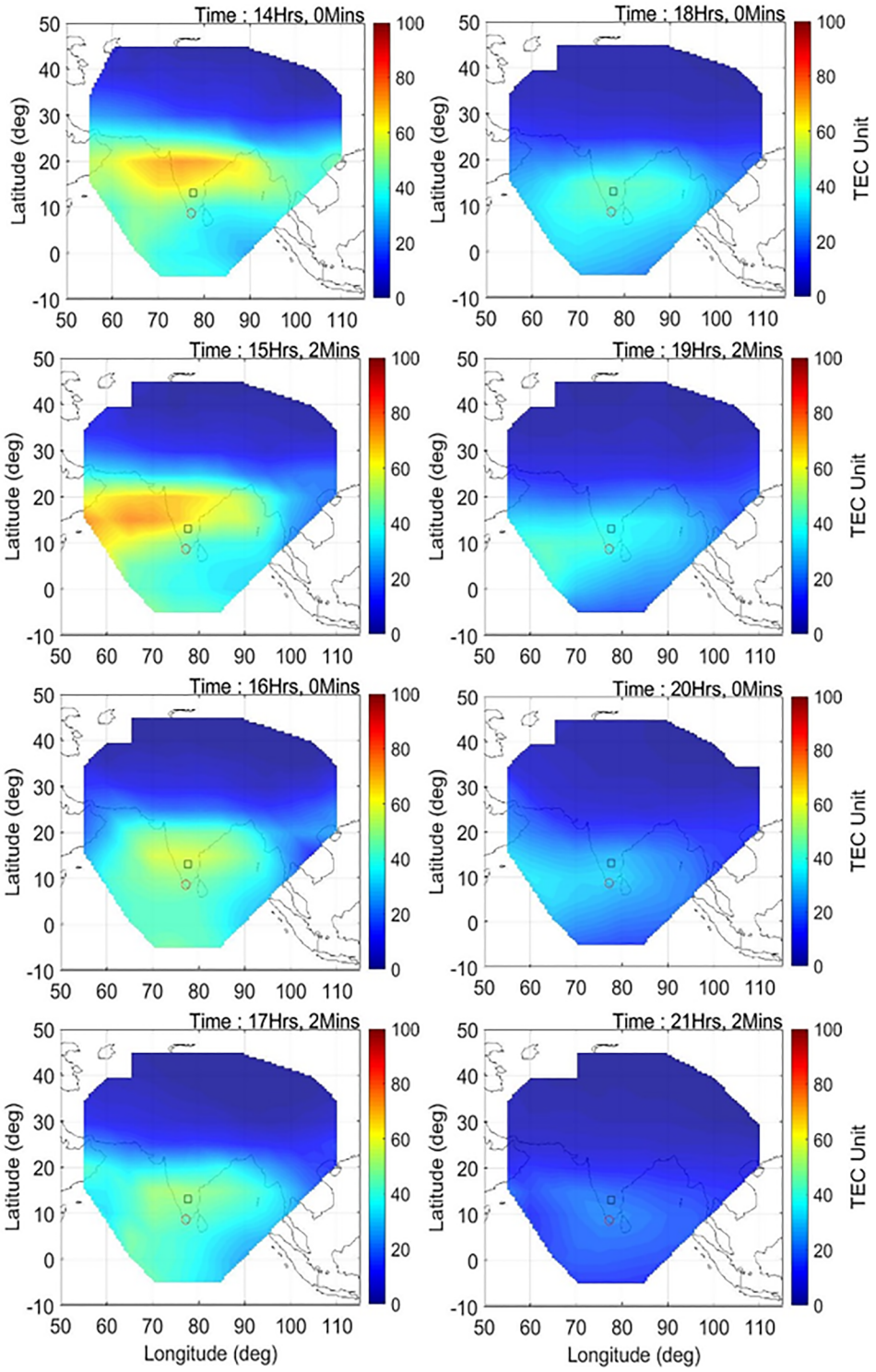

Figure 5. Same as Figure 3 but for 21 February 2014.

~15–1730 UT. Both TEC and foF2 show the peak enhancement at 18–19 UT. The large enhancement in the vertical drift at 13–14 UT indicates the prevalence of large PRE on this day. It is known that the presence of large PRE is one of the prerequisites to trigger the spread-F as observed in this case during 1530–1730 UT that lead to the absence of ionosonde derived values during this time. The vertical drift showed a sudden

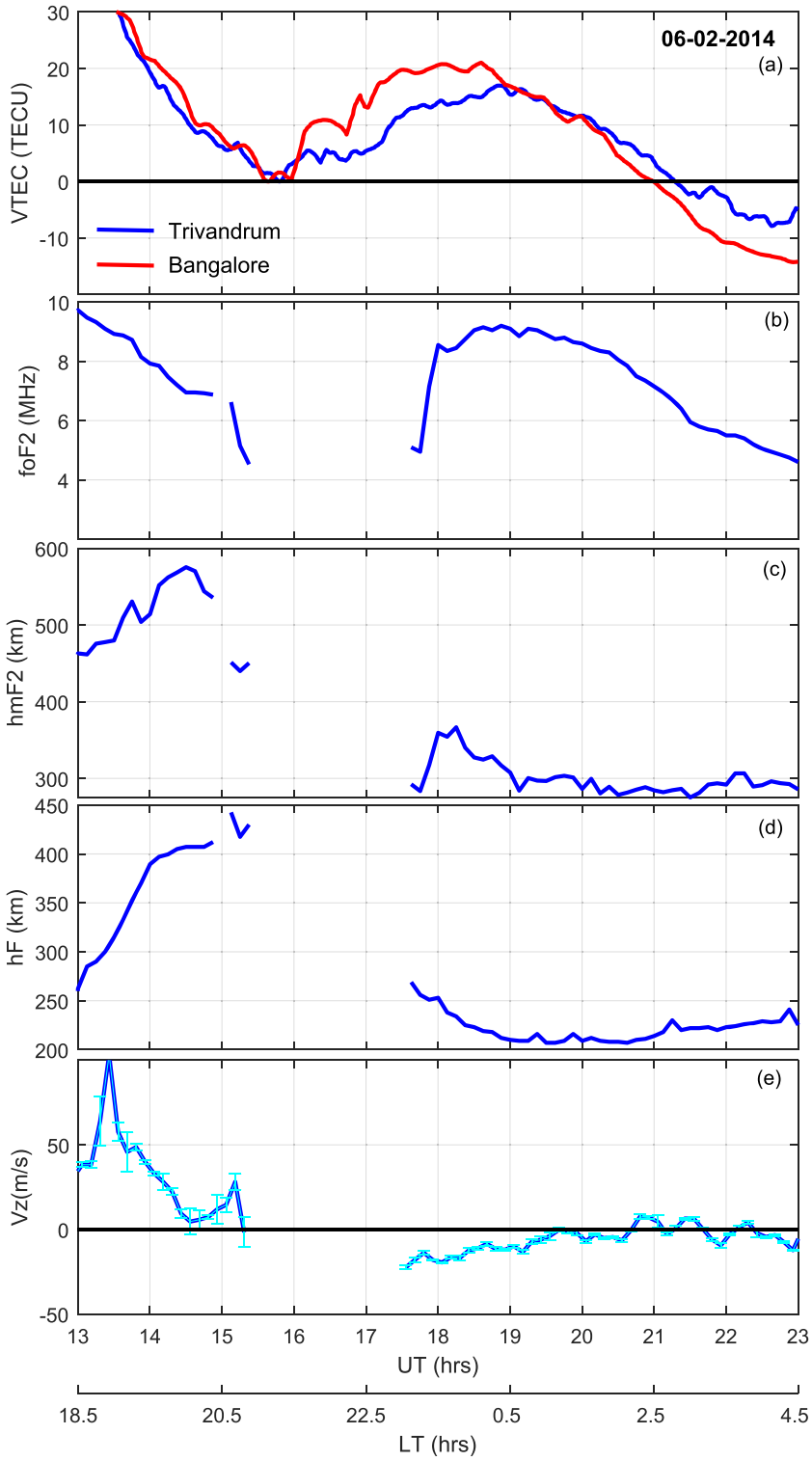

Figure 6. Same as Figure 2 but for 06 February 2014.

decrease from 14 UT, and negative values were observed at 1730–1930 UT (~ − 20 m/s). In spite of the absence of values at 1530–1730 UT, the sudden decrease in the hmF2 and h′F of about 280 and 200 km, respectively, from 15 UT to 17 UT is discernible. The abrupt decrease in the hmF2 and h′F also indicates the prevalence of the downward drift during this time.

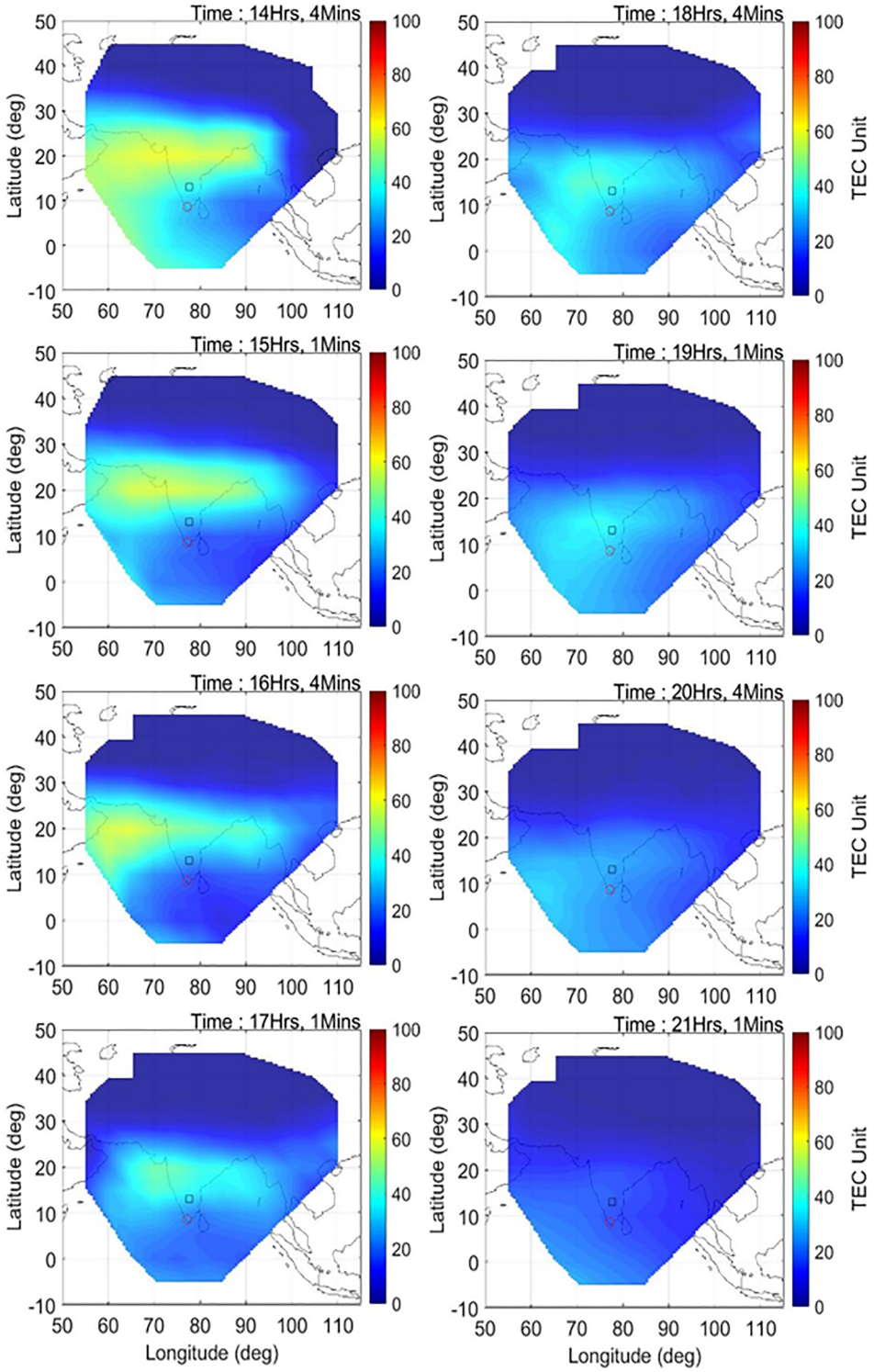

Figure 7. Same as Figure 3 but for 06 February 2014.

The presence of EIA crest and its motion can be seen from the time sequential images during 14–21 UT presented in Figure 7. The presence of large vertical drift at 13–14 UT (Figure 6) leads to the formation of evening fountain effect, which is observed in terms of strong EIA crest at 14–16 UT in the 2D-TEC maps (Figure 7) and a large depletion in the TEC values after sunset (14–16 UT) over both the equatorial

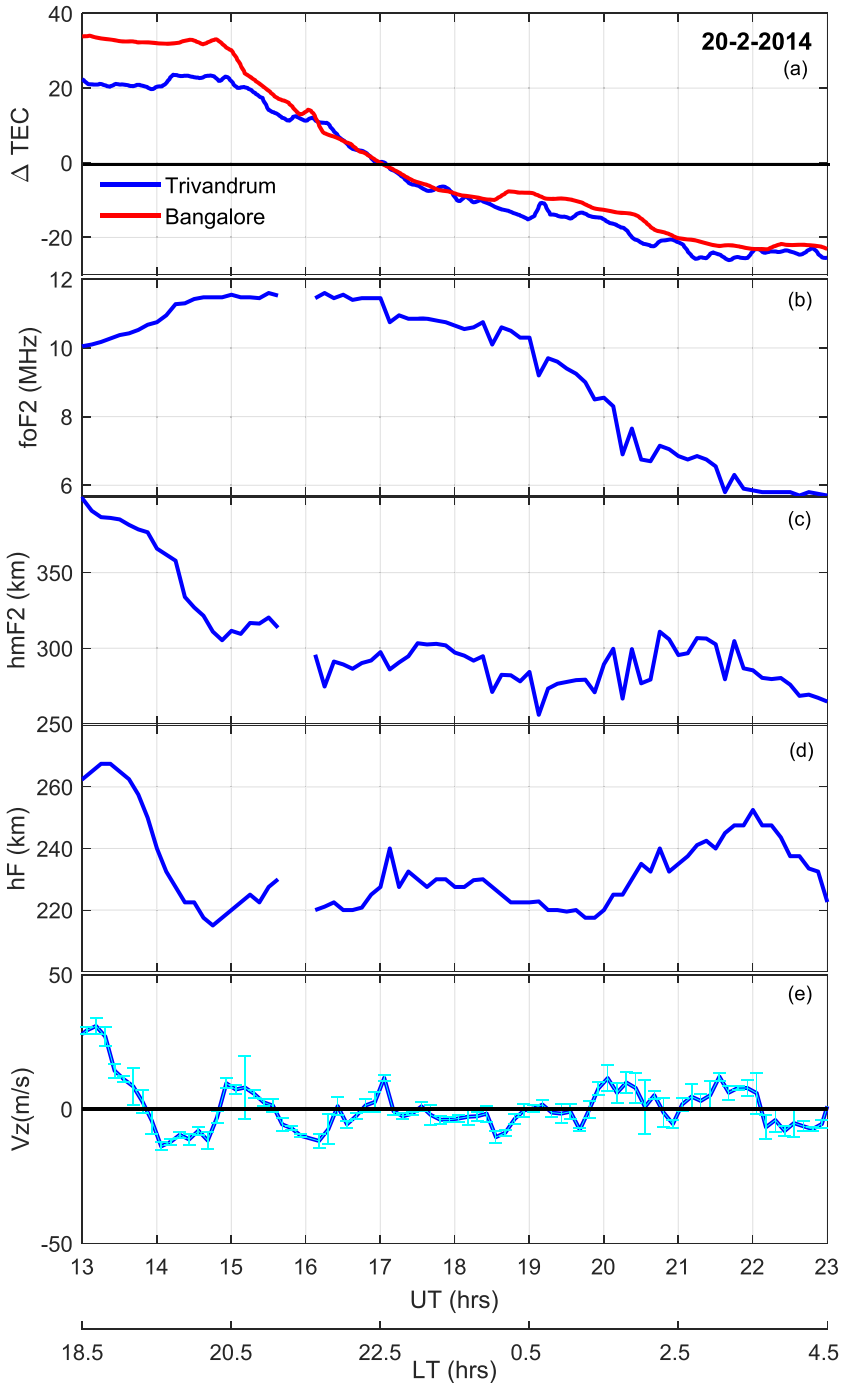

Figure 8. Same as Figure 2 but for 20 February 2014.

stations (Figure 1). The crest of ionization was observed to be restricted to 15–25°N till ~16 UT. The kind of redistribution of the EIA crest ionization as observed in the previous case (Case 2: 21 February 2014) is not observed in this case (see Figures 5 and 7). In this case (06 February 2014), the EIA crest was found to recede gradually toward the equator after ~16 UT. The increase in the ΔTEC values in Figure 6 was also observed after 16 UT. With further progression of time, EIA crest further receded in latitude and hump of ionization was observed to be located at ~10–15°N during 18–19 UT (Figure 7). It is interesting to note that the maximum enhancement in the ΔTEC values in Figure 6 was also observed nearly at the same time when the receding crest appeared at around 10°N in the 2D-TEC maps.

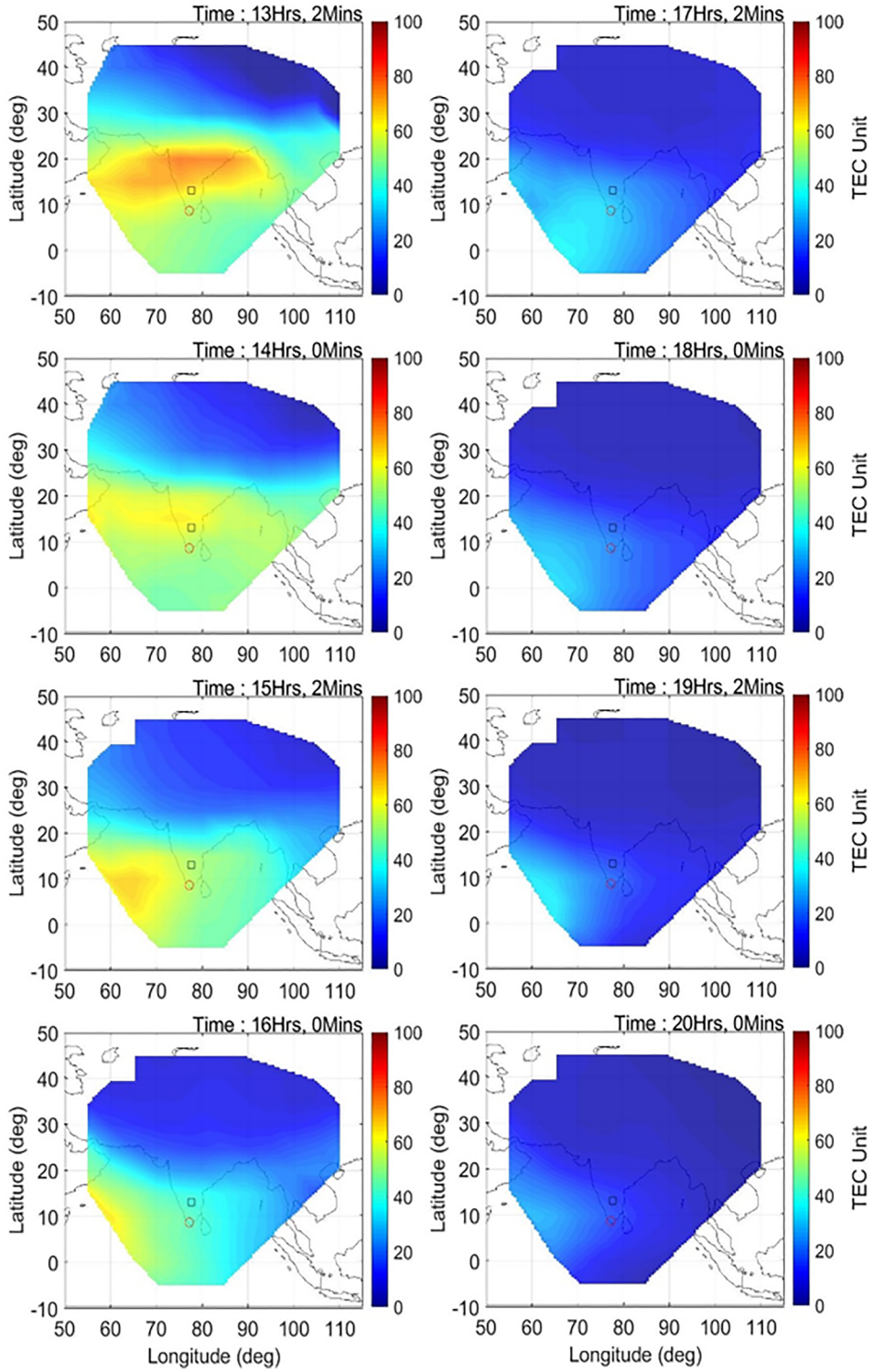

Figure 9. Same as Figure 3 but for 20 February 2014.

3.4. Case 4: 20 February 2014

In contrast to the earlier three cases, the presence of INE was absent during 20 February 2014. It can be seen from Figure 8 that the PRE which caused the height rise at ~13 UT did not cause any considerable enhancement in the ΔTEC or foF2 values during and after this time period. However, a small hump of ~5TECU was

observed in the ΔTEC values over both stations at 14–15 UT. The ΔTEC values over both stations showed a gradual decrease after 15 UT. The foF2 showed less variations and remained between ~10–12 MHz from 13 to 19 UT. After 19 UT, gradual decay in the foF2 values were observed. The h′F and hmF2 also displayed no considerable change; however, a small increase of ~20–30 km was observed during 17–18 UT and 20–22 UT. Similarly, no considerable change was observed in the vertical drift as well.

Figure 9 shows the time sequential 2D-TEC maps on 20 February 2014. It should be noted that in this case, maps are shown from 13 UT, that is, 1 hr prior to the other events. This enables highlighting the significant reduction of anomaly after 13 UT. The presence of intense EIA crest between 10°N and 25°N at 13 UT diminished at 14 UT and began to disappear from 15 UT. During this time, it is interesting to note a small hump of ~5TECU in the ΔTEC values (at 14–15 UT in Figure 8). It is clear from the 2D-TEC maps that after 15 UT, the ionization began to decrease in the region with no discernible crest of ionization. After 18 UT (2330 LT), uniform ionization prevailed over the entire region, which is completely different from the situation seen on the days when INE was observed. This behavior is reflected in the ΔTEC values with gradual decrease in the ΔTEC values after 15 UT.

4. Summary and Discussion

Although the phenomenon of INE has been of interest to the ionospheric community for the past several decades, there have been very limited studies on the INE events particularly over the equatorial regions. Based on a case study, the present work carries out a comprehensive analysis to investigate the plausible mechanism causing premidnight and postmidnight INE over the equatorial region. The 2D-TEC maps generated by using SBAS messages have been used, for the first time, to visualize the reverse fountain effect and its impact on the electron density distribution over the nighttime equatorial ionosphere. Consistent with the findings of earlier studies, present results show that the downward E × B plasma drift due to westward electric field at night is the main driving force for the INE. But the distinctive feature of our results is that they provide a direct connection between the reverse fountain effect and the INE over the equatorial region. Interestingly, the INEs over the equatorial stations occurred exactly at the time when the EIA crest as seen in the 2D-TEC maps appeared over the equatorial stations. Thus, the results not only shed light on the mechanism of INE over the equatorial and low-latitudes but also demonstrate the efficiency of 2D-TEC maps generated from SBAS to visualize the motion of EIA during nighttime and its effect on the distribution of electron density over the equatorial ionosphere.

It is well-known that EIA subsides after the sunset due to the reversal of the zonal electric field in the westward direction, creating the reverse fountain effect (e.g., Hanson & Moffet, 1966); however, observations visualizing the reverse fountain effect are rather sparse. There had been studies pertaining to the motion of EIA using TEC maps generated primarily by radio occultation technique and ionospheric tomography (Lin et al., 2007; Yeh et al., 2001). But these studies suffer from the limitation of low temporal resolution and, therefore, could not focus on the variability of the reverse fountain effect. The present study involves the use of unique SBAS-derived 2D-TEC maps to study the variability of the reverse fountain effect. These maps are available at a high temporal resolution and brought out significant day-to-day variability of the reverse fountain effect and its impact on the distribution of plasma density over the entire low latitude. For some cases, nighttime EIA crest was strong and found to be retreating gradually toward lower latitudes. The strong INE events were found to occur during such conditions. It is interesting to note that the location of the crest of anomaly as observed in the 2D-TEC maps is found to be positioned over the equatorial region during the appearance of INE over the two stations. Thus, the results highlight the importance of SBAS-derived 2D-TEC maps to visualize the motion of EIA. It is worth mentioning here that the ionospheric corrections are broadcasted in the form of vertical delay corresponding to the predefined IGPs. The SBAS-derived TEC maps correspond to the TEC values over a particular IGP. Therefore, even though the spatial resolution of these 2D-TEC maps is 5° × 5°, they are ideal for studying the motion of anomaly. On the contrary, the TEC measurements from the GPS receiver over a particular location is an integrated electron content over a large spatial area depending on the chosen elevation angle. Using the elevation angle of 45°, the spatial coverage at an ionospheric pierce point of 350 km is ~700 km. Therefore, although there exhibits a tendency of INE appearing first over Bangalore, we could not discern the exact time delay between the occurrence time of INE over the two stations.

The 2D-TEC maps provide the direct evidence to the fact that INE over equatorial region is associated with the subsidence of anomaly back toward the equator. The abrupt reduction of the crest strength along with the simultaneous increase in the ionization over the entire low latitude is one of the notable features derived from the 2D-TEC maps. This situation appears like the redistribution of crest ionization toward lower latitudes and is found to occur when the early downward drift prevailed over the equatorial region. Interestingly, the premidnight INE events were found to occur under these conditions. It can be appreciated that if the postmidnight INE is associated with the reverse fountain effect, then it should appear first over Bangalore and with a certain time lag over Trivandrum. Once the crest retreated to dip-equator, it would persist for a finite time duration before decaying due to recombination. The present results clearly demonstrate the presence of these two features as the postmidnight enhancement exhibited a tendency of occurring early over Bangalore and persisted for a longer time duration over the equatorial station, Trivandrum.

For the reverse fountain to operate, the presence of westward electric field is prerequisite, but the meridional wind might also play a key role in the formation of INE over the equatorial region. The role of meridional neutral wind in the evolution/inhibition of EIA has already been demonstrated by the previous workers (Balan et al., 1995; Balan & Bailey, 1995; Lin et al., 2007; Narayanan et al., 2013). Over equatorial and low-latitude regions of the Indian longitudes, the meridional wind was found to accelerate in the equatorward direction at ~1900–2000 IST and remained equatorward till midnight (Krishna Murthy et al., 1990; Gurubaran & Sridharan, 1993; Haridas et al., 2016). The strong equatorward meridional wind may reinforce the formation of INE by pushing the ionization around the EIA crest region toward the equator along the geomagnetic field lines. It could be construed from the above discussion that stronger equatorward wind may cause the larger INE over the equator for a given electric field or downward drift. Thus, the situation of redistribution of ionization toward the equator could also be associated with the strong equatorward meridional wind.

Using numerical simulations, Le et al. (2014) suggested that the combined effect of the westward electric field and equatorward meridional wind causes significant equatorward/downward plasma flux, which, in turn, results in a decrease of electron density at topside ionosphere, enhancement in F2 and below region, and decrease in peak height of F2 layer. The combined effect of decrease of electron density at topside ionosphere and enhancement in F2 should be reflected in TEC as it is the columnar electron content having contribution from both the topside as well as the bottomside ionosphere. The present results clearly demonstrate these features as the kind of dramatic increase seen in the nighttime foF2 values is not reflected in the TEC values (see Cases 1 and 2). In Case 1 (Figure 2), an enhancement of more that ~150% in the foF2 was noted, while it remained ~120% for the TEC. On the contrary, in Case 2 (Figure 4), continuing enhancement was observed in the foF2 values, whereas TEC showed a gradual decrease. This kind of characteristic differences in the behavior of fof2 and TEC in the nighttime equatorial ionosphere has not been shown/considered in earlier studies. The present observations provide evidence regarding the crucial role of westward electric field in deciding the behavior of nighttime foF2 and TEC over the equatorial region.

Previous studies suggested that premidnight INEs are the consequence of the PRE which raises the F region plasma to higher altitudes with reduced recombination rates and forms the premidnight enhancements in electron density at low latitudes (Zhao et al., 2008 and reference therein). Keeping this in mind, studies on INE were focused primarily on the postmidnight INE (Liu et al., 2013, Le et al., 2014; Jiang et al., 2016). However, present observations clearly indicate that the premidnight INE is not invariably associated with the PRE and can be associated with the reverse fountain effect. The previous studies also suggested that the downward $E \times B$ plasma drift due to westward electric field at night is the main driving force for the INE (Le et al., 2014; Liu et al., 2013); however, they could not provide the direct association of INE with the EIA as shown in the present study. Further, the nighttime enhancement in foF2 is also found to be accompanied by lowering of F2 layer at middle latitudes (Pirog et al., 2011). The proposed causative mechanism is entirely different over midlatitude, and it is believed to be caused by the westward electric field, which drives cross-L plasmaspheric compression. This causes an increase in the plasma pressure in the lower L-shell and enhances the downward field-aligned flux. Jiang et al. (2016) studied the postmidnight enhancement peaks in F layer electron density at low latitudes and reported that the lower the geomagnetic latitude, the earlier is the occurrence of peak enhancement. The time of occurrence of the postmidnight plasma density peak was also examined by Farelo et al. (2002), and they found that the latitudinal variation of the occurrence time of the INE peak is almost constant. Thus, the results presented by Jiang et al. (2017) and Farelo et al. (2002) are

inconsistent with the present observations. It is to be noted that Farelo et al. (2002) investigated the global morphology of nighttime NmF2 enhancements and considered stations were mostly from midlatitude. Further, Jiang et al. (2017) suggested that the combined vertical plasma drift velocity induced by the electric field and poleward meridional wind are the controlling factor for postmidnight enhancement to occur over equatorial and low-latitude stations. It is worth mentioning that their study was solely based on the ionosonde observations with a prime objective to investigate the local time of occurrence of the postmidnight enhancement peaks. On the contrary, the present observations indicate that the westward electric field (downward vertical drift) may act as a main driving force for the nighttime enhancement over equatorial region as also suggested by the previous workers, but the enhancement over these regions are associated with the retreating anomaly. Therefore, this study adds new dimensions to the study of INE over the equatorial regions by demonstrating the direct linkage between INE and reverse fountain effect.

Acknowledgments
The SBAS data used in the study are part of the GAGAN project, a joint collaboration between Airports Authority of India (AAI) and Indian Space Research Organization (ISRO). The GPS and ionosonde data from Trivandrum and Bangalore used in the paper have been collected under the INSWIM (Indian Network for Space Weather Impact Monitoring) project of Space Physics Laboratory (SPL), VSSC, ISRO. These data can be accessed directly at http://www.spl.gov.in/SPL/images/SPL-METADATA/InSWIM-MDM-DATA.zip, or alternately, the data are available at the website www.spl.gov.in/SPL. The data are posted under the INSWIM Metadata link and can be reached by clicking the Metadata link at the website. S. Y. duly acknowledges the Department of Science and Technology (DST) for the INSPIRE faculty award and the Director, Space Physics Laboratory for hosting the position. S. Y. also acknowledges NICT, Japan, for giving fellowship under NICT International Exchange Program and ISEE, Nagoya University, Japan, for hosting the position.

References

Bailey, G. J., Sellek, R., & Balan, N. (1991). The effect of interhemispheric coupling on nighttime enhancements in ionospheric total electron content during winter at solar minimum. *Annales de Geophysique*, *9*, 734–747.

Balan, N., & Bailey, G. J. (1995). Equatorial plasma fountain and its effects: Possibility of an additional layer. *Journal of Geophysical Research*, *100*(A11), 21,421–21,432. https://doi.org/10.1029/95JA01555

Balan, N., Bailey, G. J., Nair, B. B., & Titheriedge, J. E. (1994). Nighttime enhancements in ionospheric electron content in the northern and southern ionosphere. *Journal of Atmospheric and Solar - Terrestrial Physics*, *56*, 67–79. https://doi.org/10.1016/0021-9169(94)90177-5

Balan, N., & Rao, P. B. (1987). Latitudinal variations of nighttime enhancements in total electron content. *Journal of Geophysical Research*, *92*(A2), 3436–3440. https://doi.org/10.1029/JA092iA04p03436

Balan, N., et al. (1995). Modelling studies of the conjugate-hemisphere differences in ionospheric ionization at equatorial anomaly latitudes. *Journal of Atmospheric and Terrestrial Physics*, *57*(3), 279–292. https://doi.org/10.1016/0021-9169(94)E0019-J

Dabas, R. S., & Kersley, L. (2003). Study of mid-latitude nighttime enhancement in F-region electron density using tomographic images over the UK. *Annales de Geophysique*, *21*, 2323–2328.

Farelo, A. F., Herraiz, M., & Mikhailov, A. V. (2002). Global morphology of night-time NmF2 enhancements. *Annales de Geophysique*, *20*, 1795–1806.

Gurubaran, S., & Sridharan, R. (1993). Effect of meridional winds and neutral temperatures on the F layer heights over low latitudes. *Journal of Geophysical Research*, *98*(A7), 11,629–11,635.

Hanson, W. B., & Moffet, R. J. (1966). Ionization transport effects in the equatorial F region. *Journal of Geophysical Research*, *71*, 5559–5572.

Haridas, M. M., Manju, G., & Arunamani, T. (2016). Solar activity variations of nocturnal thermospheric meridional winds over Indian longitude sector. *Journal of Atmospheric and Solar-Terrestrial Physics*, *147*, 21–27. https://doi.org/10.1016/j.jastp.2016.06.010

Janve, A. V., Rai, R. K., Deshpande, M. R., Rastogi, R. G., Jain, A. R., Singh, M., & Grum, H. S. (1979). On the nighttime enhancement in ionospheric total electron content at low latitudes. *Annales Geophysicae*, *35*, 159.

Jiang, C., Chunhua, J., Chi, D., Guobin, Y., Jing, L., Peng, Z., Tatsuhiro, Y., et al. (2016). Latitudinal variation of the specific local time of postmidnight enhancement peaks in F layer electron density at low latitudes: A case study. *Journal of Geophysical Research: Space Physics*, *121*, 3476–3483. https://doi.org/10.1002/2015JA022319

Krishna Murthy, B., Hari, S., & Somayajulu, V. (1990). Nighttime equatorial thermospheric meridional winds from ionospheric h′F data. *Journal of Geophysical Research*, *95*(A4), 4307–4310. https://doi.org/10.1029/JA095iA04p04307

Le, H., Liu, L., Chen, Y., Zhang, H., & Wan, W. (2014). Modeling study of nighttime enhancements in F region electron density at low latitudes. *Journal of Geophysical Research: Space Physics*, *119*, 6648–6656. https://doi.org/10.1002/2013JA019295

Lin, C. H., Liu, J. Y., Fang, T. W., Chang, P. Y., Tsai, H. F., Chen, C. H., & Hsiao, C. C. (2007). Motions of the equatorial ionization anomaly crests imaged by FORMOSAT-3/COSMIC. *Geophysical Research Letters*, *34*, L19101. https://doi.org/10.1029/2007GL030741

Liu, L., Chen, Y., Le, H., Ning, B., Wan, W., Liu, J., & Hu, L. (2013). A case study of postmidnight enhancement in F-layer electron density over Sanya of China. *Journal of Geophysical Research: Space Physics*, *118*, 4640–4648. https://doi.org/10.1002/jgra.50422

Lois, L., Peres, H., Lazo, B., Jakowski, N., & Landrock, R. (1990). Nighttime enhancement of the F2-layer ionization over Havana, Cuba: A relationship with solar activity. *International Journal of Geomagnetism and Aeronomy*, *30*, 76–82.

Luan, X., Wang, W., Burns, A., Solomon, S. C., & Lei, J. (2008). Midlatitude nighttime enhancement in F region electron density from global COSMIC measurements under solar minimum winter condition. *Journal of Geophysical Research*, *113*, A09319. https://doi.org/10.1029/2008JA013063

Mikhailov, A. V., Förster, M., & Leschinskaya, T. Y. (2000). On the mechanism of the post-midnight winter NmF2 enhancements: Dependence on solar activity. *Annales de Geophysique*, *18*(11), 1422–1434. https://doi.org/10.1007/s00585-000-1422-y

Mikhailov, A. V., Leschinkaya, T. Y., & Förster, M. (2000). Morphology of NmF2 nighttime increases in the Eurasian sector. *Annales de Geophysique*, *18*(6), 618–628. https://doi.org/10.1007/s00585-000-0618-5

Mukherjee, G. K. (2002). Mapping of the simultaneous movement of the equatorial ionization anomaly (EIA) and ionospheric plasma bubbles through all-sky imaging of OI 630 nm emission. *Terrestrial Atmospheric and Oceanic Sciences*, *13*, 53–64.

Narayanan, V. L., Gurubaran, S., Emperumal, K., & Patil, P. T. (2013). A study on the night time equatorward movement of ionization anomaly using thermospheric airglow imaging technique. *Journal of Atmospheric and Solar - Terrestrial Physics*, *103*, 113–120. https://doi.org/10.1016/j.jastp.2013.03.028

Pavlov, A. V., & Pavlova, N. M. (2007). Anomalous night-time peaks in diurnal variations of NmF2 close to the geomagnetic equator: A statistical study. *Journal of Atmospheric and Solar - Terrestrial Physics*, *69*, 1871–1883.

Pirog, O., Deminov, M., Deminova, G., Zherebtsov, G., & Polekh, N. (2011). Peculiarities of the nighttime winter foF2 increase over Irkutsk. *Advances in Space Research*, *47*, 921–929.

Reinisch, B. W., Huang, X., Galkin, I. A., Paznukhov, V., & Kozlov (2005). Recent advances in real-time analysis of ionograms and ionospheric drift measurements with Digisondes. *Journal of Atmospheric and Solar - Terrestrial Physics*, *67*, 1054–1062. https://doi.org/10.1016/j.jastp.2005.01.009

Scali, J. L., Reinisch, B. W., Kelley, M. C., Miller, C. A., Swartz, W. E., Zhou, Q. H., & Radicella, S. (1997). Incoherent scatter radar and Digisonde observations at tropical latitudes, including conjugate point studies. *Journal of Geophysical Research*, *102*, 7357–7367.

Sridharan, R., Sekar, R., Gurubaran, S., 1993, Two-dimensional high-resolution imaging of the equatorial plasma fountain, *Journal of Atmospheric and Solar - Terrestrial Physics*, *55*, 1661–1665.

Su, Y. Z., Bailey, G. J., & Balan, N. (1994). Night-time enhancements in TEC at equatorial anomaly latitudes. *Journal of Atmospheric and Solar - Terrestrial Physics*, *56*, 1619–1628. https://doi.org/10.1016/0021-9169(94)90091-4

Sunda, S., Sridharan, R., Vyas, B. M., Khekale, P. V., Parikh, K. S., Ganeshan, A. S., et al. (2015). Satellite-based augmentation systems: A novel and cost-effective tool for ionospheric and space weather studies. *Space Weather*, *13*, 6–15. https://doi.org/10.1002/2014SW001103

Woodman, R. F., & La Hoz, C. (1976). Radar observations of F region equatorial irregularities. *Journal of Geophysical Research*, *81*(31), 5447–5466. https://doi.org/10.1029/JA081i031p05447

Yadav, S., Sunda, S., & Sridharan, R. (2016). The impact of the 17 March 2015 St. Patrick's Day storm on the evolutionary pattern of equatorial ionization anomaly over the Indian longitudes using high-resolution spatiotemporal TEC maps: New insights. *Space Weather*, *14*(10), 786–801. https://doi.org/10.1002/2016SW001408

Yeh, K. C., Franke, S. J., Andreeva, E. S., & Kunitsyn, V. E. (2001). An investigation of motions of the equatorial anomaly crest. *Geophysical Research Letters*, *28*, 4517–4520.

Young, D. M. L., Yuen, P. C., & Roelofs, T. H. (1970). Anomalous nighttime increases in total electron content. *Planetary and Space Science*, *18*, 1163–1179.

Zhao, B., Wan, W., Liu, L., Igarashi, K., Nakamura, M., Paxton, L. J., et al. (2008). Anomalous enhancement of ionospheric electron content in the Asian-Australian region during a geomagnetically quiet day. *Journal of Geophysical Research*, *113*, A11302. https://doi.org/10.1029/2007JA012987